

Polarization Sweeps in Rotation Powered Pulsars

Johann A. Hibschan^{1,2} and Jonathan Arons^{1,2,3}

*University of California, Berkeley*⁴

ABSTRACT

We re-examine the characteristic polarization angle sweep of rotation-powered pulsars and calculate the expected deviations from this sweep caused by aberrational effects and by polar-cap current flow. We find that in addition to the previously known phase shift of the entire sweep by $\Delta\Phi = -4r/R_L$, aberration shifts the polarization angle itself by $\Delta\Psi = -(10/3)(r/R_L)\cos\alpha$. Similarly, current flow above the polar cap shifts the polarization sweep by $\Delta\Psi = (10/3)(r/R_L)(J/J_{GJ})\cos\alpha$, potentially providing a method of directly measuring the magnitude of the current. The competition between these two effects produces a potentially observable signature in the polarization angle sweep. Although these effects may appear similar to orthogonal mode shifts, they are an independent phenomenon with distinct observational characteristics.

1. Introduction

The characteristic S-curve polarization sweeps exhibited by pulsar emission have spawned a large body of research, both theoretical and observational. Ever since the highly-successful rotating vector model of Radhakrishnan & Cooke (1969), hereafter RC, fitting pulsar polarization profiles has been a standard method of constraining the underlying pulsar geometry. Some pulsars, however, have polarization behavior which does not fit the standard S-curve. The millisecond pulsars, for example, seem to have noisy and on average flatter polarization sweeps than normal (Xilouris, et al. 1998). In attempts to understand these deviations, several relativistic and plasma effects have been proposed which would modify the sweep through plasma propagation effects (Barnard & Arons 1986; McKinnon 1997), through aberration of the beaming direction from strict parallelism (Blaskiewicz, Cordes, & Wasserman 1991), or through multiple interacting orthogonal modes (McKinnon & Stinebring 1998).

¹Theoretical Astrophysics Center

²Physics Department

³Astronomy Department

⁴Address correspondence to J. Hibschan, TAC, 601 Campbell, Berkeley 94720-3411. email: johann@leporello.berkeley.edu

Such effects become progressively more important as the radius of emission (or the polarization-limiting radius) approaches the light cylinder distance, $R_L \equiv c/\Omega$. r/R_L is very small in the polar cap emission model for pulsars ($r \approx R_*$), a model consistent with most observational constraints on r (Rankin 1990). Since R_L is significantly smaller for millisecond pulsars, due to their faster rotation, we expect these effects to be proportionally larger.

However, most of the departures from the pure RC model previously considered have depended on effects of second-order or higher in r/R_L , such as the field sweepback perturbation of Barnard (1986). The only first-order effect which has been considered is the aberrational shift due to the co-rotational velocity, examined by Blaskiewicz, Cordes, & Wasserman (1991), hereafter BCW. In this paper, we re-examine that effect and analyze an additional first-order effect due to current flow above the polar cap.

This is a phenomenological study, guided by the success of the rotating vector model. That model contains three chief assumptions: that the observed radiation is beamed along the direction of the magnetic field lines, that the polarization of the radiation is at a fixed angle to the radius of curvature of the field lines, as is the case for vacuum curvature radiation, and that the underlying magnetic field is a dipole. To go beyond this, we relax some of these assumptions in physically-motivated ways. Keeping the assumption that the polarization is related to the curvature of the field lines, we include aberrational change in the beaming direction and the effects of currents on the underlying dipole field.

After taking these effects into account, we find that aberration delays the phase of the polarization sweep with respect to the center of emission and, in a plot of polarization angle vs. rotation phase, shifts the entire sweep downwards, while current flow shifts the entire sweep upwards. If both effects are present, they may lead to sharp jumps in the polarization angle near the edges of current-carrying zones.

2. Polarization Perturbations

Since we assume that the polarization is related to the acceleration of the emitting particles and that the emission is beamed along the direction of motion, the particle velocity field is the core quantity examined in this paper. Particles follow the magnetic field, so any perturbations to that field are reflected in the velocity.

We apply the same general method to several perturbations. Starting with a simple dipole field, we add a perturbation to find the new velocity field of the emitting particles. From that field, we can calculate the radius-of-curvature vector of the particles at each point in space. Then, for any pulsar phase, we find the position where the velocity field at a given radius r points towards the observer, evaluate the radius of curvature vector at that point, and project it onto the sky to find the observed polarization angle.

To obtain analytic expressions, these calculations are done to first order in r/R_L . This naturally gives the difference $\Delta\psi$ between the normal polarization angle sweep, $\psi(\Phi)$ and the perturbed sweep, $\psi'(\Phi) = \psi(\Phi) + \Delta\psi(\Phi)$. More details of this procedure are given in Appendix A.

Two angles define the basic geometry of a pulsar: the angle α between the rotation axis ($\mathbf{\Omega}$) and the magnetic moment ($\mathbf{\mu}$), and the inclination angle i between the rotation axis and the line of sight to the observer ($\hat{\mathbf{\ell}}$), see Figure 1. The angle of closest approach, the minimum angle between $\mathbf{\mu}$ and $\mathbf{\Omega}$, is then $\beta \equiv i - \alpha$.

These calculations are done in magnetic-centered coordinates, defined so that the z axis ($\theta = 0$) is along the magnetic moment $\mathbf{\mu}$, the rotation axis $\mathbf{\Omega}$ is fixed in the $x - z$ ($\phi = 0$) plane, and the vector to the observer $\hat{\mathbf{\ell}}$ is also in the $x - z$ plane at $t = 0$.

We have also numerically calculated the expected polarization angle sweeps for each perturbation examined. Given a modified velocity field, we directly solved for the new emission point, computed the radius of curvature vector, and compared it to the rotation axis to find a polarization angle. These numerical results confirmed the analytic perturbation theory.

2.1. Offset dipoles

One suggested perturbation to the magnetic field is an offset dipole, where the center of the dipolar field is offset from the center of the star, e.g. Chen & Ruderman (1993). This has negligible effect on the polarization sweep. In an offset dipole, the magnetic origin revolves about the center of the neutron star with a radius of $\delta < R_*$. In turn, in the frame of the magnetic field, the observer appears to move in a circle of identical radius. The electrodynamics in these field-centered coordinates is the same as in the star-centered case, so the only change in the observed emission is that due to the effective motion of the observer. This motion and the resultant changes are tiny, on the order of $\delta/d \ll 1$, where d is the distance to the observer.

2.2. Polar Field Aligned Current

Most models of the pulsar polar cap include a current of charged particles streaming along the field lines, a current approximately equal to the Goldreich-Julian density moving at the speed of light. This current induces a magnetic field of $\mathbf{B}_1 = (r/R_L)(J/J_{GJ})B \cos \alpha \hat{\mathbf{e}}_\phi$; this field is purely toroidal with respect to the magnetic axis.

From Appendix D, the resulting polarization angle shift is

$$\Delta\psi = \frac{10}{3} \frac{r}{R_L} \frac{J}{J_{GJ}} \cos \alpha \left(1 - \frac{7}{40} \sin^2 \theta_0 \right) \text{ radians} \quad (1)$$

where θ_0 is the magnetic colatitude of the (0^{th} -order) emission point, see Appendix B. At the

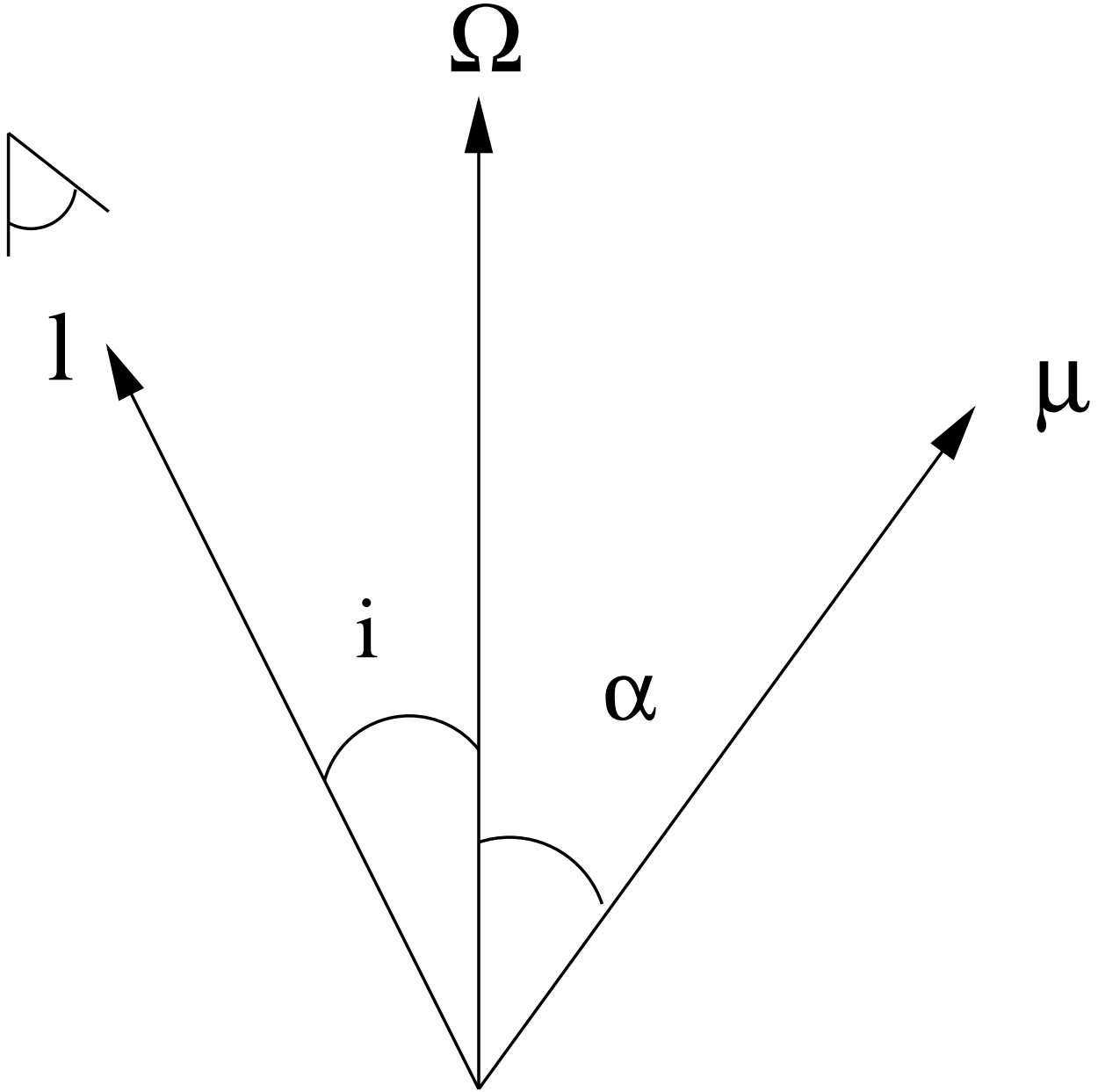


Fig. 1.— Basic Angles. α is the angle between the rotation axis, Ω , and the magnetic moment, μ . i is the angle between the observer LOS, ℓ , and the rotation axis.

center of the pulse, θ_0 has its minimum value, $\theta_0 \approx (2/3)|\alpha - i| = (2/3)|\beta|$. At the boundary of the last closed field line, θ_0 reaches its maximum, $\theta_0 \approx (2/3)\sqrt{r/R_L}$. For r/R_L small, the range of θ_0 is also small, and the perturbation is mostly flat across the observed pulse.

In terms of the orbital phase, the perturbation is

$$\Delta\psi \approx \frac{10}{3} \frac{r}{R_L} \frac{J}{J_{GJ}} \cos \alpha \left(\frac{27}{32} + \frac{5}{32} \cos \beta \right) - \frac{25}{192} \frac{r}{R_L} \frac{J}{J_{GJ}} \sin 2\alpha \sin i \sin^2 \Omega t. \quad (2)$$

To get this form, we used the approximation formulae of Appendix C, assumed that Ωt was small enough that $\cos \Omega t \approx 1 - (1/2) \sin^2 \Omega t$, and simplified the constants by taking $28/45 \approx 5/8$, which is good to 0.4%. Here, $t = 0$ corresponds to the center of the pulse profile, where the slope of the polarization angle curve is greatest.

In terms of observables, $r/R_L \approx 1.2^\circ P_{0.1}^{-1} r_{100}$, where r_{100} is the emission radius in units of 100 km and $P_{0.1}$ is the pulse period in units of 0.1 seconds, so the magnitude of this shift is $4.0^\circ P_{0.1}^{-1} (J/J_{GJ}) r_{100}$.

2.3. Aberration

As discussed by Blaskiewicz, Cordes, & Wasserman (1991), the rotation of the magnetosphere itself affects the velocities of particles moving along field lines. Inside the light cylinder, the field lines are stationary in the frame co-rotating with the star. However, as particles move along these lines, their paths curve both because of the curvature of the field line itself and because the frame of those field lines rotates with the star. Even if the field lines were straight, the paths of the particles moving along them would be helices in the inertial frame. This extra curvature generates a perturbation of the instantaneous particle directions equal to the co-rotation velocity, $\mathbf{\Omega} \times \mathbf{r}$.

To lowest order, this perturbation shifts the polarization angle by

$$\Delta\psi = -2 \frac{r}{R_L} \frac{\sin \alpha \cos \phi_0}{\sin \theta_0} + O\left(\frac{r}{R_L}\right). \quad (3)$$

Since $\sin \theta_0$ is generally tiny, on the order of the polar cap size, $\theta_c \equiv \sqrt{r/R_L}$, this perturbation is of order $\sqrt{r/R_L}$, a half-order lower than the constant shift produced by the current.

This shift has the same form as a phase shift of the entire polarization sweep by

$$\Delta\Phi = -3 \frac{r}{R_L} \quad (4)$$

with respect to the geometric center of the pulse phase, as was found previously by BCW. Since aberration advances the emission itself by $\Delta\Phi = r/R_L$ due to simple beaming, the total phase shift with respect to the emission is $\Delta\Phi = -4r/R_L$.

From numerical investigations, representing this effect as a phase shift closely matches the perturbation. The analytic method presented here only gives the first order correction (in r/R_L)

to the sweep; higher-order terms quickly become important, since aberration adds appreciable curvature to central field lines which formerly had none. Representing the change as a phase shift better reflects these higher-order terms, while giving the same first-order result.

If Figure 3, we show the numerically-calculated polarization sweep for $r/R_L = 0.1$; this gives a good idea of the character of the perturbation. As shown in Figure 4, when $r/R_L = 0.01$, the analytically predicted first-order shift is nearly identical to the numerical, while at $r/R_L = 0.1$ there is a noticeable difference between the two, which is mostly corrected by casting the perturbation as a phase shift.

Once this phase shift is removed, we are left with a remaining perturbation of

$$\Delta\Psi = -\frac{10}{3}\frac{r}{R_L}\cos\alpha\left(1 - \frac{7}{10}\sin^2\theta_0\right) + \frac{47}{12}\frac{r}{R_L}\sin\alpha\sin\theta_0\cos\phi_0 + O(\sin^3\theta_0). \quad (5)$$

See Appendix G for details. In terms of the pulsar phase, this is approximately

$$\Delta\Psi \approx -\frac{10}{3}\frac{r}{R_L}\cos\alpha\left(\frac{3}{8} + \frac{5}{8}\cos\beta\right) + \frac{47}{18}\frac{r}{R_L}\sin\alpha\sin\beta - \frac{23}{144}\frac{r}{R_L}\sin 2\alpha\sin i\sin^2\Omega t \quad (6)$$

using the same approximations as for Eq. (2).

The constant portion of this polarization angle shift cancels the constant portion of the perturbation due to polar current flow when $J/J_{GJ} = 1$. However, if $J/J_{GJ} \neq 1$, there is a nonzero shift, providing a diagnostic of the magnitude of current flow. The remaining linear and quadratic terms produce slight changes to the shape of the polarization angle sweep.

2.4. Relativistic Sweep-back

The actual magnetic field of a pulsar will differ from the ideal dipole due to the relativistic sweep-back of field lines, caused by the induced displacement current. The full vacuum fields are given in Deutsch (1955) and most recently restated by Melatos (1997). Admittedly, the region surrounding a pulsar is almost certainly not a vacuum, but the morphology of the vacuum field should roughly reflect the structure of the magnetic field with conduction currents.

The difference between the Deutsch fields and the vacuum dipole is *second* order in r/R_L , however, so the first order effects considered here dominate at low altitudes ($r/R_L < 0.2$).

In the non-vacuum case, the corresponding perturbation is the magnetic field due to the rotation of the Goldreich-Julian density. This field component satisfies $\nabla \times \mathbf{B}_{rot} = 4\pi(\mathbf{\Omega} \times \mathbf{r}/c)\eta_{GJ}$. Since both $\mathbf{\Omega} \times \mathbf{r}/c$ and $r\eta_{GJ}/B_0$ are manifestly first-order in r/R_L , B_{rot}/B_0 is second order and therefore has been neglected.

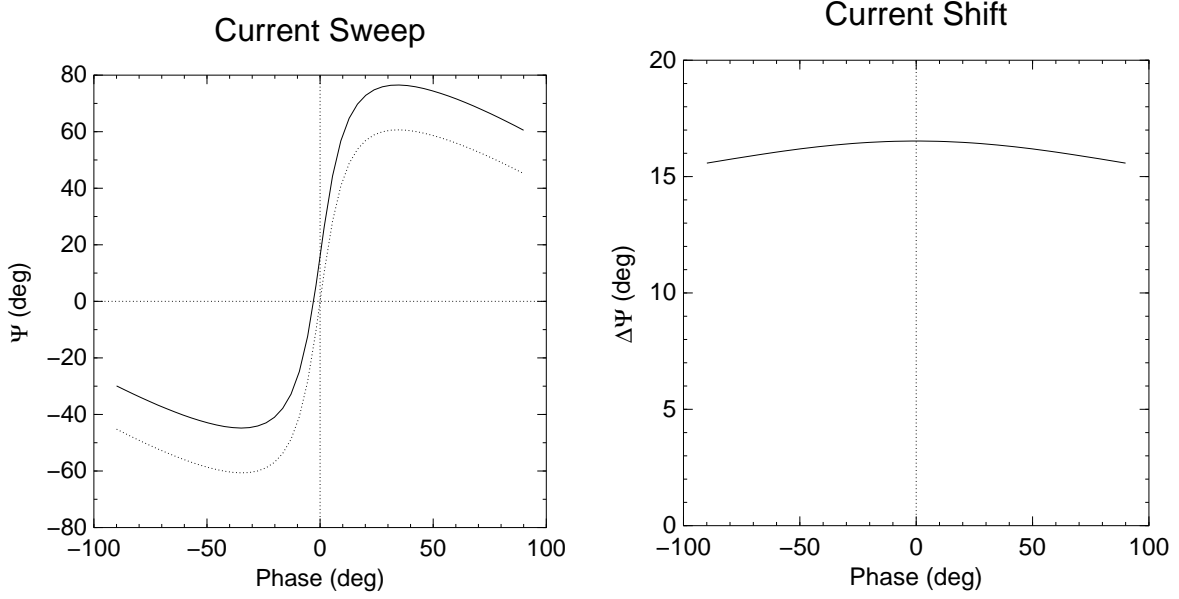


Fig. 2.— Perturbation to polarization angle, $\Delta\psi$, due to a Goldreich-Julian current as a function of longitude. All angles are in degrees. The dotted line is the unperturbed sweep, while the solid line is the perturbed sweep. $r/R_L = 0.1$, $\alpha = 30^\circ$, and $i = 35^\circ$.

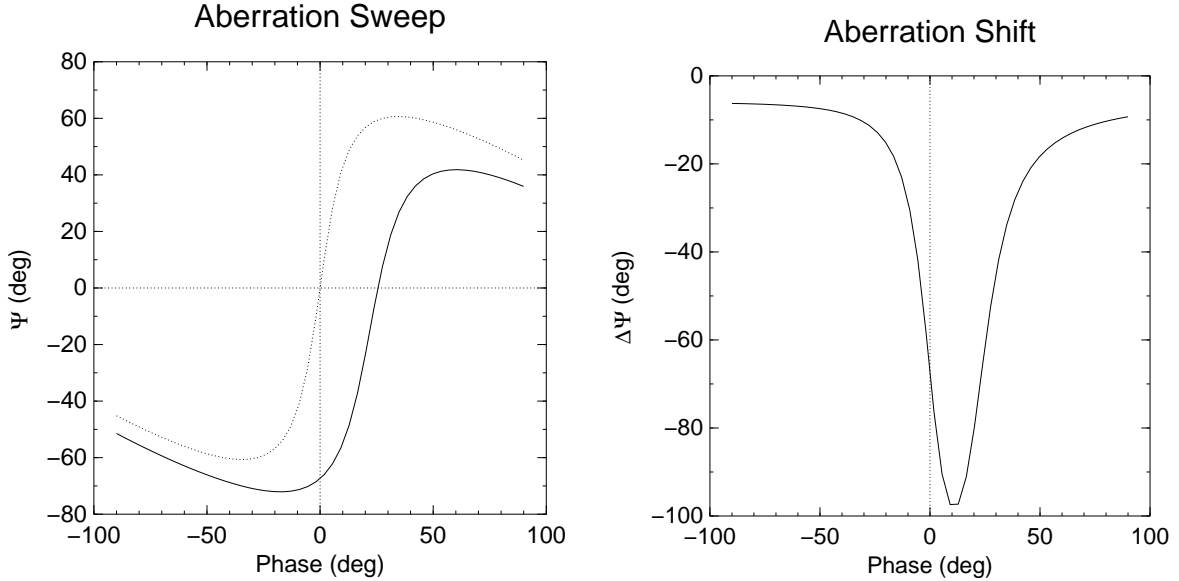


Fig. 3.— Perturbation to polarization angle, $\Delta\psi$, due to co-rotation effects as a function of longitude. All angles are in degrees. The dotted line is the unperturbed sweep, while the solid line is the perturbed sweep. $r/R_L = 0.1$, $\alpha = 30^\circ$, and $i = 35^\circ$.

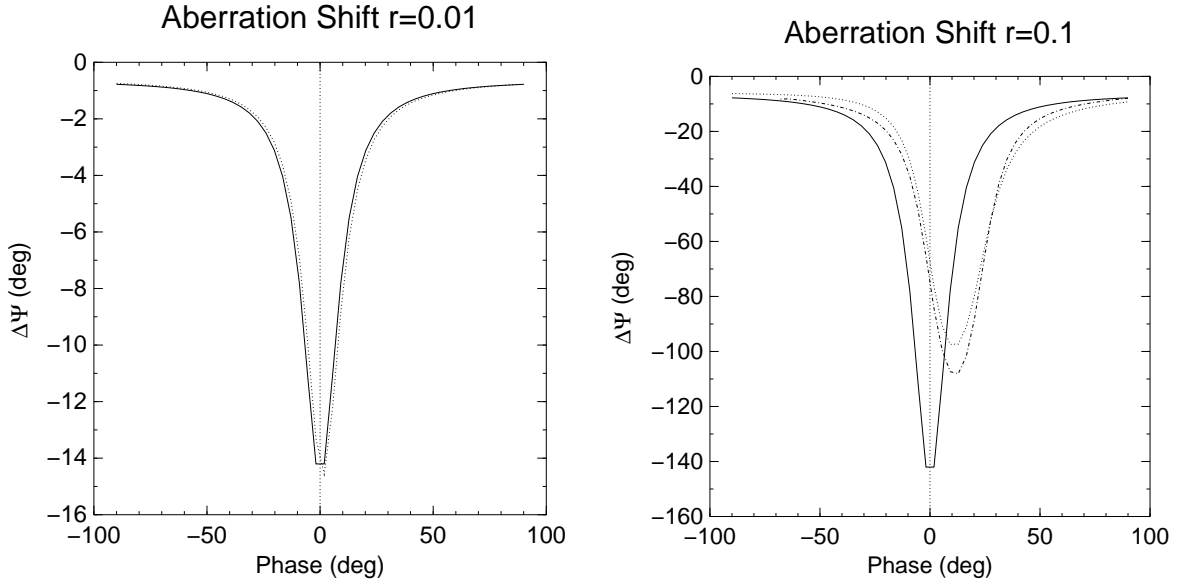


Fig. 4.— Analytic polarization angle shift due to aberration compared to the numerical for $r/R_L = 0.01$ and $r/R_L = 0.1$. $\alpha = 30^\circ$, and $i = 35^\circ$. The solid line is the analytic perturbation theory, the dot-dash line (for $r/R_L = 0.1$) is the phase shift derived from the perturbation theory, and the dotted line is the numerical result. Casting the perturbation as a phase shift better matches the numerical result for large r/R_L .

3. Return Currents

While the perturbations described in the previous section are general effects, this section applies those effects to a specific model of the polar cap. To maintain charge balance, the current flowing out from the polar cap must be balanced by a return current elsewhere in the system. Here, we assume this current flows along the boundary layer of last-closed field lines, surrounding the polar cone (Goldreich and Julian 1969).

Outside this auroral sheath, the net current flow through a loop surrounding the pole is zero, so there is no magnetic field perturbation due to the current. Only the aberrational shift remains. The field on the open field lines stays the same, containing perturbations from both current and aberration, while within the layer itself the current perturbation is quickly eliminated. For more detailed analytic models, see Appendix E.

If this return current layer is illuminated by emission, it will produce a characteristic signature in the polarization sweep, Figure 5. The sharp transitions are caused by the current perturbation turning on and off as the line of sight passes through the return current layer.

Although the return current layer is not normally thought of as a site of emission, it may be visible either through direct emission, by some form of two-stream instability, or through refraction or scattering of radiation emitted within the cone. Since we are more interested in the consequences of current flow above polar caps, we leave the precise mechanism of the emission open. If the return current is composed of outflowing positrons or ions, the beaming properties would be much the same as those of the primary beam, while if the return current interpenetrates the outflow, even the identical mechanism would reflect the presence of the return current. Transitions like the one in Figure 5 would be strong evidence for emission in this region or radiation transfer through it.

In addition to these specific effects, a more general conclusion is that inhomogeneities on the order of J_{GJ} in the current flow above pulsar polar caps should produce perturbations in the polarization angle sweep on the order of r/R_L .

4. Discussion

Given a single polarization angle sweep, at a single frequency, observers can hope to see the effects of any current inhomogeneities, small deviations from the standard shape caused by higher-order terms, and the phase shift between the center of the polarization angle sweep and the pulse itself. The constant offsets caused by current flow would be detectable only through comparison of multiple frequencies, which would also help confirm any of the other effects.

From a more qualitative point of view, these concepts may be used to help understand certain difficult objects. For example, the potentially large jumps in the polarization angle when the line of sight crosses a return current layer could explain some of the shifts which are normally ascribed

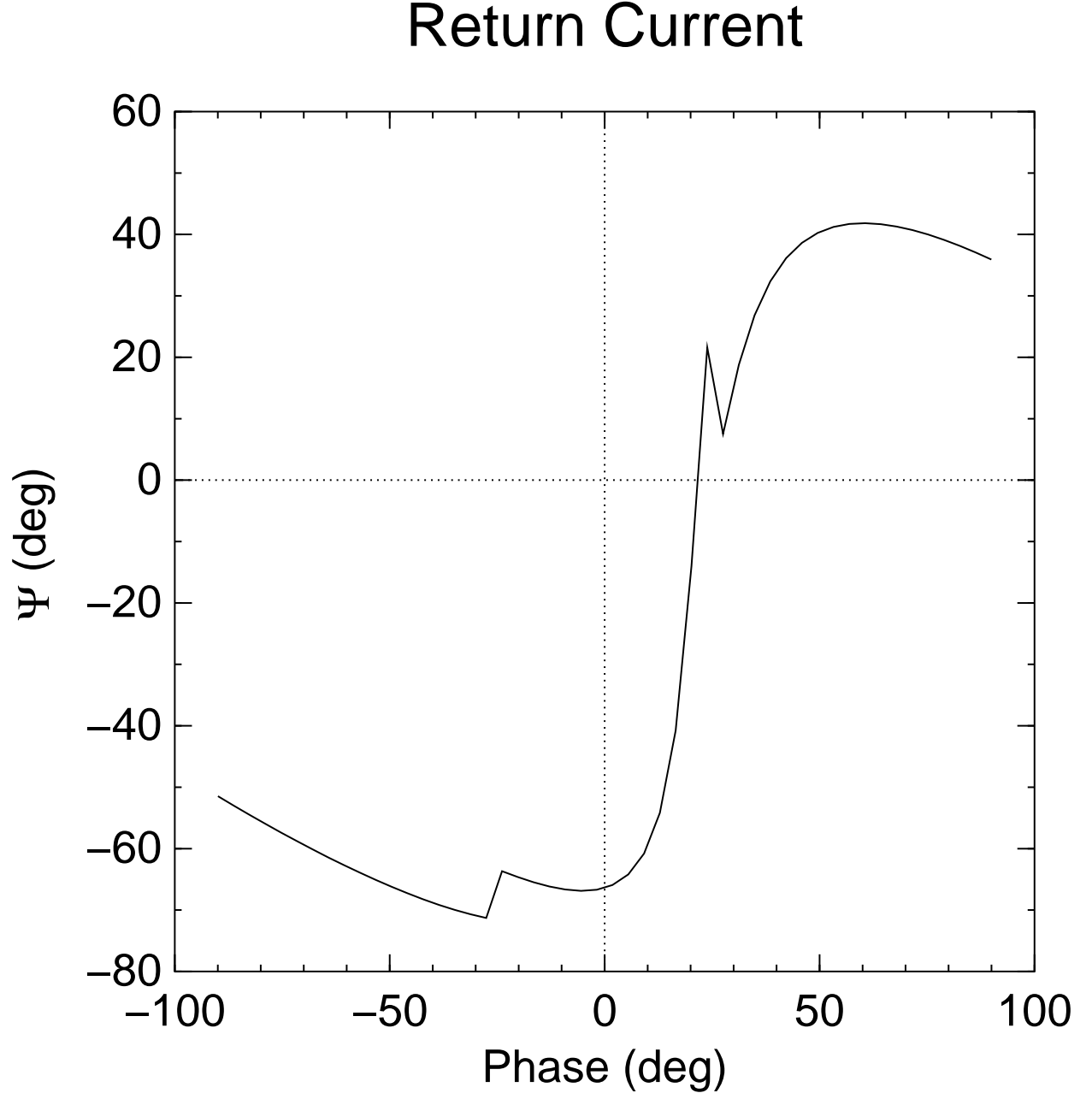


Fig. 5.— Polarization sweep for $\alpha = 30^\circ$, $i = 35^\circ$, and $r/R_L = 0.1$, with a return current layer at $\Phi = \pm 25^\circ$ with a thickness set by $\lambda = 50$, showing the resultant jumps in the polarization angle sweep.

to orthogonal modes. Clearly, this result does not explain orthogonal modes in general, as can be seen from the single-pulse studies of XXX, but these shifts could masquerade as orthogonal mode transitions in individual pulsars.

For example, in J0437-0415, the magnitude of the “orthogonal” transitions changes with frequency, ranging from 90° at high frequency to 70° and 40° at lower frequencies, suggesting that either these are orthogonal modes combined with propagation effects or, perhaps, that the 90° shift is a coincidence and these shifts are instead due to current features in the magnetosphere.

In addition to polarization jumps, J0437-0415 displays a polarization phase lag in which higher frequencies lag lower (Navarro 1997). Combined with the increasing transition amplitude with frequency, this suggests that the higher frequencies arise from higher in the magnetosphere than the lower frequencies, contrary to the normal radius-to-frequency map. Since most millisecond pulsars do not display the pulse widening with decreased frequency that is one of the best arguments for radius-to-frequency mapping in normal pulsars, it is certainly conceivable that the structure of the emission region is different. In any case, the small range of phase shifts seen argues for a small emission region, on the order of a few kilometers.

5. Summary

In this paper, we have shown how two physical effects, rotational aberration and current flow, affect the polarization angle of observed radiation. The strength of these effects is proportional to the height of the emission region.

In brief, current flow tends to shift the entire polarization angle sweep upwards in a plot of polarization angle vs. phase, while aberration tends both to shift the sweep downwards and to phase shift it. The largest of these is the aberrational phase shift between the center of the emission profile and the center of the polarization sweep.

The Goldreich-Julian current and aberration produce equal and opposite constant offsets to the polarization angle sweep, effectively cancelling each other. Any deviations in the current from the fiducial Goldreich-Julian value will break this cancellation, giving a potential indicator of the magnitude of current flow above the polar cap.

Inhomogeneities in the current flow structure above the polar cap should be revealed as perturbations, of order r/R_L , in the polarization sweep. The specific case of an auroral return current layer would appear as sharp transitions along the edge of the observed pulse, potentially correlated with conal emission. These jumps may appear similar to orthogonal modes, but should have an amplitude which changes with frequency, if frequency is related to emission radius. In the presence of current sheets, single-pulse polarimetry should show a shift in both orthogonal modes, provided that multiple altitudes do not contribute to the observed radiation at one frequency. This is quite different from the existing single-pulse studies (Gil & Lyne 1995; Gangadhara 1997), which show a

simple shift in the relative amplitude of two existing modes.

We would like to thank Don Backer and Andrea Somer for illuminating discussions about the observability of these effects and Anatoly Spitkovsky for helpful animations of swept-back field lines.

A. Geometric Method

From classical differential geometry, the tangent vector is the unit vector along \mathbf{B} , $\hat{\mathbf{t}} = \mathbf{B}/|\mathbf{B}|$, while the normal vector $\hat{\mathbf{n}}$ is the unit vector along the radius of curvature. For highly relativistic flow, radiation is beamed along the direction of the particle velocity, so at any instant the observed radiation comes from the spot in the magnetosphere where the tangent vector $\hat{\mathbf{t}}$ points in the direction of the observer.

For normal vacuum radiation, the polarization vector must lie in the plane perpendicular to $\hat{\mathbf{t}}$; for the particular case of curvature radiation, the polarization is almost entirely along $\hat{\mathbf{n}}$. For plasma processes, this restriction is relaxed, but in the absence of other directional perturbations, such as density gradients not along $\hat{\mathbf{n}}$, we expect that the polarization angle would be related to the direction of curvature of the field lines. Density gradients along $\hat{\mathbf{n}}$, which we expect if polar cap pair creation is the main source of the plasma, would likewise link the polarization to the magnetic geometry.

To trace the orientation of the field, we use the binormal vector, defined by $\mathbf{b} \equiv \hat{\mathbf{t}} \times \hat{\mathbf{n}}$. This is equivalent to tracing the normal, but is computationally more convenient, since the binormal of a dipole field is simply a constant vector along \mathbf{e}_ϕ .

The observed polarization angle is then set by finding the angle between the normal vector and the projected rotation axis of the pulsar. Since the tangent points towards the observer, both the normal and the binormal are automatically in the plane of the sky, but the rotation axis must be projected, giving $\boldsymbol{\Omega}_p \equiv \hat{\boldsymbol{\Omega}} - (\hat{\boldsymbol{\Omega}} \cdot \hat{\mathbf{t}})\hat{\mathbf{t}}$.

If the angle between the rotation axis and the binormal is ψ' , then $\cos \psi' = \hat{\mathbf{b}} \cdot \hat{\boldsymbol{\Omega}}_p$ and $\sin \psi' = \hat{\mathbf{t}} \cdot (\hat{\mathbf{b}} \times \hat{\boldsymbol{\Omega}}_p)$. Since the angle made by the normal vector is 90° different from that made by the binormal, the true polarization angle is given by

$$\tan \psi = -\cot \psi' = \frac{\hat{\mathbf{b}} \cdot \hat{\boldsymbol{\Omega}}}{\hat{\mathbf{b}} \cdot (\hat{\mathbf{t}} \times \hat{\boldsymbol{\Omega}})} \quad (\text{A1})$$

where we have expressed the result in terms of $\hat{\boldsymbol{\Omega}}$, rather than $\boldsymbol{\Omega}_p$.

For a standard dipole field, this gives the normal polarization curve,

$$\tan \psi = \frac{\sin \alpha \sin \Omega t}{\cos \alpha \sin i - \sin \alpha \cos i \cos \Omega t}, \quad (\text{A2})$$

c.f. Radhakrishnan & Cooke (1969).

In general, we want to know the change in the polarization angle due to a small perturbation to the background magnetic field, $\mathbf{B} = \mathbf{B}_0 + \mathbf{B}_1$. This change is due to shifts in both the emission point and the binormal itself.

To first order, the new tangent vector $\hat{\mathbf{t}}$ will be the sum of the initial tangent vector, $\hat{\mathbf{t}}_0$, and a perturbation \mathbf{t}_1 perpendicular to $\hat{\mathbf{t}}_0$. (Any component along $\hat{\mathbf{t}}_0$ is simply absorbed into the normalization.)

The new curvature vector is

$$\boldsymbol{\kappa} = (\hat{\mathbf{t}} \cdot \nabla) \hat{\mathbf{t}} = (\hat{\mathbf{t}}_0 \cdot \nabla) \hat{\mathbf{t}}_0 + (\hat{\mathbf{t}}_0 \cdot \nabla) \mathbf{t}_1 + (\mathbf{t}_1 \cdot \nabla) \hat{\mathbf{t}}_0 = \boldsymbol{\kappa}_0 + \boldsymbol{\kappa}_1 \quad (\text{A3})$$

where $\boldsymbol{\kappa} \equiv \hat{\mathbf{n}}/\rho$, $\boldsymbol{\kappa}_0 = \hat{\mathbf{n}}_0/\rho_0 = (\hat{\mathbf{t}}_0 \cdot \nabla) \hat{\mathbf{t}}_0$, and

$$\boldsymbol{\kappa}_1 = (\hat{\mathbf{t}}_0 \cdot \nabla) \mathbf{t}_1 + (\mathbf{t}_1 \cdot \nabla) \hat{\mathbf{t}}_0 \quad (\text{A4})$$

When normalized, the component of $\boldsymbol{\kappa}_1$ along $\hat{\mathbf{n}}_0$ is absorbed into the normalization, giving a perturbed normal vector of $\hat{\mathbf{n}} = \hat{\mathbf{n}}_0 + \mathbf{n}_1$, where

$$\mathbf{n}_1 = \rho_0(\boldsymbol{\kappa}_1 - (\hat{\mathbf{n}}_0 \cdot \boldsymbol{\kappa}_1) \hat{\mathbf{n}}_0). \quad (\text{A5})$$

The perturbed binormal is then $\hat{\mathbf{b}} = \hat{\mathbf{b}}_0 + \mathbf{b}_1$, where

$$\mathbf{b}_1 = \mathbf{t}_1 \times \hat{\mathbf{n}}_0 + \hat{\mathbf{t}}_0 \times \mathbf{n}_1. \quad (\text{A6})$$

The second contribution to the polarization angle change comes from the change in the emission point. If the unperturbed field points towards the observer at \mathbf{r}_0 , the perturbed does so at $\mathbf{r}_0 + \mathbf{r}_1$, where \mathbf{r}_1 can be found by solving

$$\hat{\mathbf{t}}_0(\mathbf{r}_0) + \nabla \hat{\mathbf{t}}_0 \cdot \mathbf{r}_1 + \mathbf{t}_1(\mathbf{r}_0) = \hat{\boldsymbol{\ell}} \quad (\text{A7})$$

or

$$\mathbf{r}_1 = -[\nabla \hat{\mathbf{t}}_0]^{-1} \cdot \mathbf{t}_1(\mathbf{r}_0) \quad (\text{A8})$$

This expression is underdetermined, as there is typically an entire line of points where the field points towards the observer.

In this paper, we assume that emission at a given frequency arises at (or decouples from the magnetic field at) a fixed radius, so we constrain the radius to remain constant. This “lateral” motion shifts the emission site to a different field line from the unperturbed one, and, if transverse gradients are steep, with a size scale shorter than roughly $r^2 \sin \theta / R_L$, this will likely affect the emission properties. Near the boundaries of the polar cap, such transverse gradients may become important, requiring a more careful treatment.

This changes the observed binormal by an additional $\delta\mathbf{b} = \nabla\hat{\mathbf{b}}_0 \cdot \mathbf{r}_1$, giving a total change of $\Delta\mathbf{b} = \mathbf{b}_1 + \delta\mathbf{b}$. Since this change in the binormal is perpendicular to the unperturbed binormal, the magnitude of the change in polarization angle is simply $|\Delta\psi| = |\Delta\mathbf{b}|$.

Getting the sign correct requires comparing the change in the binormal to the direction of the projected rotation axis, or

$$\Delta\psi = \frac{\hat{\mathbf{t}}_0 \cdot (\Delta\mathbf{b} \times \Omega_p)}{\hat{\mathbf{b}}_0 \cdot \Omega_p}. \quad (\text{A9})$$

Since all of these steps are linear in the perturbation, multiple perturbations may be considered separately, then simply added. In later sections, we consider in turn two different possible perturbations to the basic dipole field.

B. Unperturbed Field

In (r, θ, ϕ) polar coordinates centered on the magnetic axis, the unperturbed dipole field is

$$\mathbf{B}_0 = \left[\frac{2\mu \cos \theta}{r^3}, \frac{\mu \sin \theta}{r^3}, 0 \right] \quad (\text{B1})$$

which gives a tangent vector field of

$$\hat{\mathbf{t}}_0 \equiv \frac{\mathbf{B}_0}{|\mathbf{B}_0|} = \frac{1}{N_1} \left[\cos \theta, \frac{1}{2} \sin \theta, 0 \right] \quad (\text{B2})$$

where

$$N_1 \equiv \left(1 - \frac{3}{4} \sin^2 \theta \right)^{1/2} \quad (\text{B3})$$

The curvature vector is then

$$\boldsymbol{\kappa}_0 \equiv (\hat{\mathbf{t}}_0 \cdot \nabla) \hat{\mathbf{t}}_0 = \frac{3 \sin \theta}{4 r N_1^4} \left(1 - \frac{1}{2} \sin^2 \theta \right) \left[-\frac{1}{2} \sin \theta, \cos \theta, 0 \right], \quad (\text{B4})$$

giving a normal vector of

$$\hat{\mathbf{n}}_0 \equiv \frac{\boldsymbol{\kappa}_0}{|\boldsymbol{\kappa}_0|} = \frac{1}{N_1} \left[-\frac{1}{2} \sin \theta, \cos \theta, 0 \right]. \quad (\text{B5})$$

The binormal is purely in the ϕ -direction,

$$\hat{\mathbf{b}}_0 = \hat{\mathbf{t}}_0 \times \hat{\mathbf{n}}_0 = [0, 0, 1]. \quad (\text{B6})$$

In order to relate this binormal field to the actual polarization angle, we need to know the emission point, which we denote $\mathbf{r}_0 = (r_0, \theta_0, \phi_0)$, where the magnetic field points towards the observer at $(\theta_{obs}, \phi_{obs})$.

Since the dipole field contains no ϕ -component, we must have $\phi_0 = \phi_{obs}$. Solving for θ_0 then gives

$$\tan \theta_0 = \frac{3}{2} \frac{1}{\tan \theta_{obs}} \left\{ \pm \left(1 + \frac{8}{9} \tan^2 \theta_{obs} \right)^{1/2} - 1 \right\} \quad (\text{B7})$$

If θ_{obs} is small, as is usually the case for an observer looking down the cone of open field lines, this simplifies to $\theta_0 \approx (2/3)\theta_{obs}$.

If we take these results and evaluate expression (A1), we obtain the standard polarization angle sweep, (A2).

C. Approximations

Evaluating the polarization effects of various perturbations naturally leads to expressions which depend on the coordinates of the emission point, usually in the frame co-rotating with the star. Since no actual observer is sitting in that co-rotating frame, we have to rewrite the results in terms of observables, such as the rotational phase (Ωt) and the physical inclination angles (α, i). Admittedly, the inclination angles are not directly observable, but they set the geometry of the pulsar.

Unfortunately, this conversion is a significant source of error in the analytic perturbation theory. Straightforward power-series expansions may be used to cast the raw analytical expressions into more useful forms, but doing so limits the range of validity to a small portion of the pulse phase near the pulse center.

Here, we first give the exact formulae relating the pulse phase to the position of the observer in these coordinates. These, coupled with the solution for the 0-order emission colatitude (B7), give a precise definition for θ_0 and ϕ_0 at any pulse phase. We then give several more tractable, but more limited, approximations.

The vector to the observer is

$$\hat{\ell} = \begin{bmatrix} \cos \alpha \sin i \cos \Omega t - \sin \alpha \cos i \\ - \sin i \sin \Omega t \\ \sin \alpha \sin i \cos \Omega t + \cos \alpha \cos i \end{bmatrix} \quad (\text{C1})$$

in Cartesian magnetic coordinates. In polar, the observer is at $(\theta_{obs}, \phi_{obs})$ given by

$$\cos \theta_{obs} = \cos \alpha \cos i + \sin \alpha \sin i \cos \Omega t \quad (\text{C2})$$

$$\tan \phi_{obs} = \frac{\sin i \sin \Omega t}{\sin \alpha \cos i - \cos \alpha \sin i \cos \Omega t}. \quad (\text{C3})$$

These expressions, coupled with (B7) and the fact that $\phi_0 = \phi_{obs}$, fully define the emission coordinates.

For emission from within the cone of open field lines, several of these angles are small. If the observer is to see this cone, the difference between α and i must be less than (or on the order of) the colatitude of the last closed field line, $\theta_c(r) = \sqrt{r/R_L}$. Similarly, the magnetic colatitude of the emission, θ_0 , and the rotational phase $\Phi = \Omega t$ must be of this same order.

The expression for $\tan \theta_0$ (B7) is perhaps the most difficult formula. It has two roots, and the continuous physical solution switches between them when $\theta_{obs} = \pi/2$. Since the maximum of θ_{obs} is $\alpha + i$, this switch will occur somewhere in the pulse phase for all pulsars with $\alpha + i > \pi/2$. If we are only interested in the region close to the pulse center, then this is not a problem, but for millisecond pulsars and other pulsars whose emission covers a substantial fraction of the period, this switch-over has to be kept in mind.

Here, however, for simplicity we assume that θ_{obs} is always less than $\pi/2$. In that case, an excellent approximation to (B7) is

$$\tan \theta_0 \approx \frac{3}{2} \frac{1}{\sin \theta_{obs}} \left(1 - \cos \theta_{obs} - \frac{1}{18} \sin^2 \theta_{obs} \right) \quad (C4)$$

while for small θ_{obs} ,

$$\tan \theta_0 \approx \sin \theta_0 \approx \frac{2}{3} \sin \theta_{obs} \quad (C5)$$

Expressing $\sin \theta_{obs}$ in terms of $\cos \theta_{obs}$ gives us, for small θ_{obs} ,

$$\sin \theta_{obs} = [2(1 - \cos \theta_{obs})]^{1/2} \quad (C6)$$

which is quite useful, since we frequently have terms in even powers of $\sin \theta_0$, and we know $\cos \theta_{obs}$ from Eq. (C2).

The observer and emission azimuth are the same, $\phi_0 = \phi_{obs}$. Using the transformed y-coordinate, $y_B = r \sin \theta \cos \phi$, we find

$$\cos \phi_0 = \frac{\cos \alpha \sin i \cos \Omega t - \sin \alpha \cos i}{\sin \theta_{obs}} \quad (C7)$$

$$\sin \phi_0 = \frac{-\sin i \sin \Omega t}{\sin \theta_{obs}} \quad (C8)$$

By using the relations between $\sin \theta_0$ and $\sin \theta_{obs}$, these can be cast into various useful forms.

For example, in order to simplify expressions (2) and (6), we used these relations to write

$$\sin^2 \theta_0 \approx \frac{4}{9} \sin^2 \theta_{obs} \approx \frac{4}{9} \left(1 - \cos \beta + \frac{1}{2} \sin \alpha \sin i \sin^2 \Omega t \right) \quad (C9)$$

and

$$\sin \theta_0 \cos \phi_0 \approx \frac{2}{3} \sin \theta_{obs} \cos \phi_{obs} \approx \frac{2}{3} \left(\sin \beta - \frac{1}{2} \cos \alpha \sin i \sin^2 \Omega t \right) \quad (C10)$$

where $\beta \equiv i - \alpha$ and we have taken $\cos \Omega t \approx 1 - (1/2) \sin^2 \Omega t$. As mentioned before, this limits these expressions to apply only to the region close to the pole where θ_{obs} is small.

D. Field Aligned Current

We expect a current to flow along the open field lines with intensity approximately equal to the Goldreich-Julian charge density moving at the speed of light,

$$\mathbf{J} = -\frac{1}{2\pi}\zeta(\boldsymbol{\Omega} \cdot \mathbf{B})\hat{\mathbf{B}} \quad (\text{D1})$$

where $\zeta = J/J_{GJ}$ is scale factor of order unity, reflecting our ignorance of the actual current. Since we will be examining only first-order effects, the results for the perturbing fields and the polarization shifts are simply proportional to ζ . In the interest of conciseness, we set $\zeta = 1$ for the rest of this section and reinsert it into the final result.

In the case of a small polar cap, the variation in $\boldsymbol{\Omega} \cdot \mathbf{B}$ across the cap is also small, so we take $\boldsymbol{\Omega} \cdot \mathbf{B} \approx \Omega B \cos \alpha$. In addition, if $\mathbf{B} = \mathbf{B}_0 + \mathbf{B}_1$, with $B_1 \ll B_0$ and $\nabla \times \mathbf{B}_0 = 0$, as is true for any superposition of vacuum multipoles, then $\nabla \times \mathbf{B}_1 = 2\Omega_* \mathbf{B}_0/c$.

Now assume \mathbf{B}_0 is a point dipole and introduce spherical polar coordinates with the z axis along the dipole axis and the origin of coordinates at the point dipole. Assume axisymmetry with respect to the magnetic axis. Since the assumed current is axisymmetric, this assumption is equivalent to assuming the polar flow tube has a circular cross section.

The equations for the field components are

$$\frac{1}{r \sin \theta} \frac{\partial}{\partial \theta} (B_{1\phi} \sin \theta) = -\frac{4\Omega_* \mu}{cr^3} \cos \alpha \cos \theta, \quad (\text{D2})$$

$$-\frac{1}{r} \frac{\partial}{\partial r} (r B_{1\phi}) = -\frac{2\Omega_* \mu}{cr^3} \cos \alpha \sin \theta, \quad (\text{D3})$$

$$\frac{1}{r} \frac{\partial}{\partial r} (r B_{1\theta}) - \frac{1}{r} \frac{\partial B_{1r}}{\partial \theta} = 0. \quad (\text{D4})$$

Here $B_{0r} = (2\mu/r^3) \cos \theta$, $B_{0\theta} = (\mu/r^3) \sin \theta$. The solution is

$$B_{1r} = B_{1\theta} = 0, \quad (\text{D5})$$

$$B_{1\phi} = -\frac{2\mu}{R_L^3} \cos \alpha \left(\frac{r}{R_L} \right)^{-2} \sin \theta, \quad (\text{D6})$$

where $R_L \equiv c/\Omega_*$. One readily finds this $B_{1\phi}$ satisfies both of the non-trivial equations.

This gives a perturbation to the tangent vector of

$$\mathbf{t}_1 = \left[0, 0, -\frac{r}{R_L} \cos \alpha \frac{\sin \theta}{N_1} \right] \quad (\text{D7})$$

in (r, θ, ϕ) polar components.

Following the above method, and expanding in powers of $\sin \theta$, the updated normal is

$$\mathbf{n}_1 = \left[0, 0, -4\frac{r}{R_L} \cos \alpha \left(1 - \frac{1}{4} \sin^2 \theta \right) \right] \quad (\text{D8})$$

which results in a change in the binormal of

$$\mathbf{b}_1 = \frac{r}{R_L} \cos \alpha \left[-\sin \theta, 4\left(1 - \frac{1}{4} \sin^2 \theta\right), 0 \right]. \quad (\text{D9})$$

The emission point changes by

$$\mathbf{r}_1 = -[\nabla \hat{\mathbf{t}}_0]^{-1} \cdot \mathbf{t}_1 = \frac{r^2}{R_L} \cos \alpha \left[0, 0, \frac{2}{3} N_1 \tan \theta \right], \quad (\text{D10})$$

changing the observed binormal by

$$\delta \mathbf{b} = \nabla \hat{\mathbf{b}}_0 \cdot \mathbf{r}_1 = -\frac{r}{R_L} \cos \alpha \left[\frac{2}{3} \sin \theta, \frac{2}{3}, 0 \right] \quad (\text{D11})$$

giving a total perturbation of

$$\Delta \mathbf{b} = \mathbf{b}_1 + \delta \mathbf{b} = \frac{r}{R_L} \cos \alpha \left[-\frac{5}{3} \sin \theta, \frac{10}{3} - \sin^2 \theta \right] \quad (\text{D12})$$

yielding a polarization angle shift of

$$\Delta \psi = \frac{10}{3} \frac{r}{R_L} \frac{J}{J_{GJ}} \cos \alpha \left(1 - \frac{7}{40} \sin^2 \theta \right), \quad (\text{D13})$$

where we have re-inserted the dependence on the current strength.

E. Return Current

To model a return current, we assume that each field line has a fixed flux of current on it, proportional to the local GJ density.

If the perturbing current density has the form

$$\mathbf{J} = -\frac{1}{2\pi} \Omega \cos \alpha \mathbf{B} f\left(\frac{\sin^2 \theta}{r}\right) \quad (\text{E1})$$

for f an arbitrary function, then the perturbing field is

$$B_{1\phi} = -\frac{2\Omega\mu}{c} \cos \alpha \frac{1}{r \sin \theta} \int_0^u du' f(u') \quad (\text{E2})$$

where $u \equiv \sin^2 \theta / r$ labels an individual field line. This is equivalent to using the magnetic flux as the integration variable.

Dividing by the magnitude of the field gives

$$\mathbf{t}_1 = \frac{\mathbf{B}_1}{|B_0|} = -\frac{\cos \alpha}{N_1} \frac{r}{R_L} \frac{r}{\sin \theta} \int_0^u du' f(u') \mathbf{e}_\phi \quad (\text{E3})$$

with N_1 as defined in (B3).

If $f(u) = 1$, we get the normal perturbing field. If we include a return current which is a multiple λ of the background GJ current in a small ring past $\sin^2 \theta / r = u_1$, namely

$$f(u) = \begin{cases} 1, & \text{if } u_1 > u > 0; \\ -\lambda, & \text{if } (1 + 1/\lambda)u_1 > u > u_1; \\ 0, & \text{if } u > (1 + 1/\lambda)u_1; \end{cases} \quad (\text{E4})$$

we get a perturbation of

$$\mathbf{t}_1 = \frac{r}{R_L} \cos \alpha \mathbf{e}_\phi \begin{cases} -\sin \theta, & \text{if } u_1 > u > 0 \\ -\frac{(1+\lambda)ru_1}{\sin \theta} + \lambda \sin \theta, & \text{if } (1 + 1/\lambda)u_1 > u > u_1 \\ 0, & \text{if } u > (1 + 1/\lambda)u_1 \end{cases} \quad (\text{E5})$$

This generates the normal polarization angle shift for $u < u_1$, no shift for $u > (1 + 1/\lambda)u_1$, and a shift of

$$\Delta\psi = \frac{10}{3} \frac{r}{R_L} \lambda \cos \alpha \left(\frac{1 + \lambda}{\lambda} \frac{u_1 r}{\sin^2 \theta} - 1 \right) \left(1 - \frac{7}{40} \sin^2 \theta \right) \quad (\text{E6})$$

for $(1 + 1/\lambda)u_1 > u > u_1$. If $\lambda \gg 1$, then this reduces to

$$\Delta\psi = -\frac{10}{3} \frac{r}{R_L} \cos \alpha (1 - \xi) \left(1 - \frac{7}{40} \sin^2 \theta \right) \quad (\text{E7})$$

where $\xi \equiv \lambda(u - u_1)/u_1$ ranges from 0 to 1 through the return current layer.

This simply eliminates the perturbation over the range from $(1 + 1/\lambda)u_1 > u > u_1$, which is what we expected. If the return current layer is thin, $\lambda \gg 1$, this transition is abrupt. This would appear in the data as a constant negative shift outside of the region of current flow, as there would no longer be any current to offset the aberration, as shown in Figure 5.

F. Aberration

The aberrational perturbation arises because the velocity of particles streaming along field lines has components both along the rotation direction and along the field line. Following Blaskiewicz, Cordes, & Wasserman (1991), the velocity of the particles becomes

$$\mathbf{v} = c\beta_{\parallel} \hat{\mathbf{B}} + \boldsymbol{\Omega} \times \mathbf{r}, \quad (\text{F1})$$

where β_{\parallel} is a free parameter, reflecting the fraction of particle velocity along the field. Assuming the particles are moving at c and normalizing gives a change in the tangent vector of

$$\mathbf{t}_1 = \frac{\boldsymbol{\Omega} \times \mathbf{r}}{c} - \left(\frac{\boldsymbol{\Omega} \times \mathbf{r}}{c} \cdot \hat{\mathbf{t}}_0 \right) \hat{\mathbf{t}}_0 \quad (\text{F2})$$

This change in the tangent vector is of the same form as the current aberration treated previously, i.e. first-order in r/R_L and perpendicular to $\hat{\mathbf{t}}_0$. As such we can apply the same general formalism to calculate the expected polarization angle shift. Additional first-order changes to the magnetic field generate second-order changes in \mathbf{t}_1 , so we may safely treat this perturbation independently.

In polar coordinates,

$$\hat{\boldsymbol{\Omega}} \times \hat{\mathbf{r}} = [0, \sin \alpha \sin \phi, \sin \alpha \cos \theta \cos \phi + \cos \alpha \sin \theta] \quad (\text{F3})$$

Subtracting out the component along \mathbf{t}_0 gives

$$\mathbf{t}_1 = \frac{r}{R_L} \begin{bmatrix} -\frac{1}{2} N_1^{-2} \sin \alpha \sin \theta \cos \theta \sin \phi \\ N_1^{-2} \sin \alpha \cos^2 \theta \sin \phi \\ \sin \alpha \cos \theta \cos \phi + \cos \alpha \sin \theta \end{bmatrix}. \quad (\text{F4})$$

Aberrational effects change the curvature of particle orbits in two ways. Not only does the instantaneous velocity of the particles change by $\boldsymbol{\Omega} \times \mathbf{r}$, but the underlying magnetic dipole is rotating as well. This adds a $\partial \mathbf{t}_0 / \partial t$ term to the curvature vector perturbation $\boldsymbol{\kappa}_1$ from (A4), giving

$$\boldsymbol{\kappa}_1 = \frac{\partial \mathbf{t}_0}{\partial t} + (\mathbf{t}_0 \cdot \nabla) \mathbf{t}_1 + (\mathbf{t}_1 \cdot \nabla) \mathbf{t}_0 \quad (\text{F5})$$

The normal vector is then found from (A5) to be

$$\mathbf{n}_1 = \frac{r}{R_L} \begin{bmatrix} -\sin \alpha \sin \phi \left(1 - \frac{1}{4} \sin^2 \theta\right) \\ -\frac{1}{2} \sin \alpha \sin \theta \sin \phi \\ \frac{8}{3} \frac{\sin \alpha \cos \phi}{\sin \theta} \left(1 - \frac{7}{4} \sin^2 \theta\right) + 4 \cos \alpha \left(1 - \frac{3}{4} \sin^2 \theta\right) \end{bmatrix} + O(\sin^3 \theta) \quad (\text{F6})$$

producing a binormal change of

$$\mathbf{b}_1 = \frac{r}{R_L} \begin{bmatrix} \frac{1}{3} \sin \alpha \cos \phi \left(1 - \frac{29}{8} \sin^2 \theta\right) + \cos \alpha \sin \theta \\ -\frac{8}{3} \frac{\sin \alpha \cos \phi}{\sin \theta} \left(1 - \frac{27}{16} \sin^2 \theta\right) - 4 \cos \alpha \left(1 - \frac{3}{4} \sin^2 \theta\right) \\ 0 \end{bmatrix} + O(\sin^3 \theta) \quad (\text{F7})$$

Solving for the emission point gives

$$\mathbf{r}_1 = \frac{r^2}{R_L} \begin{bmatrix} 0 \\ -\frac{2}{3} \sin \alpha \sin \phi \left(1 - \frac{3}{8} \sin^2 \theta\right) \\ -\frac{2}{3} \sin \alpha \cos \phi \left(1 - \frac{3}{8} \sin^2 \theta\right) - \frac{2}{3} \cos \alpha \sin \theta \end{bmatrix} + O(\sin^3 \theta) \quad (\text{F8})$$

and a change in binormal of

$$\delta \mathbf{b} = \frac{r}{R_L} \begin{bmatrix} \frac{2}{3} \sin \alpha \cos \phi \left(1 - \frac{3}{8} \sin^2 \theta\right) + \frac{2}{3} \cos \alpha \sin \theta \\ \frac{2}{3} \frac{\sin \alpha \cos \phi}{\sin \theta} \left(1 - \frac{7}{8} \sin^2 \theta\right) + \frac{2}{3} \cos \alpha \\ 0 \end{bmatrix} + O(\sin^3 \theta) \quad (\text{F9})$$

giving a total change in the binormal of

$$\Delta \mathbf{b} = \frac{r}{R_L} \begin{bmatrix} \sin \alpha \cos \phi \left(1 - \frac{35}{24} \sin^2 \theta\right) + \frac{5}{3} \cos \alpha \sin \theta \\ -2 \frac{\sin \alpha \cos \phi}{\sin \theta} \left(1 - \frac{47}{24} \sin^2 \theta\right) - \frac{10}{3} \cos \alpha \left(1 - \frac{33}{40} \sin^2 \theta\right) \\ 0 \end{bmatrix} + O(\sin^3 \theta) \quad (\text{F10})$$

and a shift in the polarization angle of

$$\Delta \psi = -2 \frac{r}{R_L} \frac{\sin \alpha \cos \phi}{\sin \theta} \left(1 - \frac{11}{6} \sin^2 \theta\right) - \frac{10}{3} \frac{r}{R_L} \cos \alpha \left(1 - \frac{7}{10} \sin^2 \theta\right) + O(\sin^3 \theta). \quad (\text{F11})$$

G. Aberrational Phase Shift

Qualitatively, the changes to the polarization angle caused by aberration appear to simply shift the phase of the sweep. BCW directly converted their calculated perturbation into a phase shift, but here we want to be slightly more precise and preserve the higher-order terms (in $\sin \theta$). A portion of the aberrational change in the binormal $\Delta \mathbf{b}$ (F10) corresponds to a phase shift, but part of it does not. In order to separate these two parts, we need to calculate how the binormal at the emission point changes with time.

This will let us decompose the perturbation into $\Delta \mathbf{b} = \Delta \Phi (\partial \mathbf{b} / \partial \Phi) + \Delta \mathbf{b}'$, which corresponds to a perturbed polarization sweep of $\psi = \psi_0(\Phi + \Delta \Phi) + \Delta \psi'$, where $\psi_0(\Phi)$ is the standard sweep, $\Delta \psi'$ is calculated from $\Delta \mathbf{b}'$ as before, and $\Phi \equiv \Omega t$.

As the star rotates, the zeroth-order binormal (as evaluated in magnetic coordinates) changes both because of the apparent motion of the observer across the sky and because of the change in the rotating coordinates themselves. The change in the binormal is

$$\frac{d\hat{\mathbf{b}}}{dt} = \frac{db^i}{dt} \mathbf{e}_i + b^i \frac{d\mathbf{e}_i}{dt} = \frac{d\hat{\mathbf{b}}^{(1)}}{dt} + \frac{d\hat{\mathbf{b}}^{(2)}}{dt} \quad (\text{G1})$$

The first term depends on the motion of the emission point in magnetic coordinates. In these coordinates, the zeroth-order binormal only depends on the azimuth of the emission point, $\phi_0 = \phi_{obs}$. From (C3), this changes in time as

$$\frac{d\phi_0}{dt} = -\Omega(\cos \alpha + \sin \alpha \cos \phi_0 \cot \theta_{obs}). \quad (\text{G2})$$

Solving for θ_{obs} in terms of θ_0 gives

$$\cot \theta_{obs} = \frac{2 - \tan^2 \theta_0}{3 \tan \theta_0} \approx \frac{2}{3} \frac{1 - \sin^2 \theta_0}{\sin \theta_0} + O(\sin^3 \theta) \quad (\text{G3})$$

The change in binormal as seen in the rotating frame is then

$$\frac{d\hat{\mathbf{b}}^{(1)}}{dt} = \frac{\partial \hat{\mathbf{b}}}{\partial \phi_0} \frac{d\phi_0}{dt} = [-\sin \theta_0, -\cos \theta_0, 0] \frac{d\phi_0}{dt} \quad (\text{G4})$$

$$= \Omega \begin{bmatrix} \frac{2}{3} \sin \alpha \cos \phi_0 (1 - \sin^2 \theta_0) + \cos \alpha \sin \theta_0 \\ \frac{2}{3} \frac{\sin \alpha \cos \phi_0}{\sin \theta_0} (1 - \frac{3}{2} \sin^2 \theta_0) + \cos \alpha (1 - \frac{3}{2} \sin^2 \theta_0) \\ 0 \end{bmatrix} + O(\sin^3 \theta_0) \quad (\text{G5})$$

where we have expanded up to third order in $\sin \theta_0$.

The second term depends on the rotation of the coordinate system. Defining $R_y(a), R_z(b)$ to be respectively rotations around the y, z axes by angles a, b , this becomes

$$\frac{d\hat{\mathbf{b}}^{(2)}}{dt} = R_y(\alpha) R_z(\Omega t) \frac{dR_z(-\Omega t)}{dt} R_y(-\alpha) \hat{\mathbf{b}} \quad (\text{G6})$$

or

$$\frac{d\hat{\mathbf{b}}^{(2)}}{dt} = \Omega [-\sin \alpha \cos \theta \cos \phi - \cos \alpha \sin \theta, -\cos \alpha \cos \theta + \sin \alpha \sin \theta \cos \phi, 0] \quad (\text{G7})$$

Adding these two and expanding to third order in $\sin \theta$ gives

$$\frac{d\hat{\mathbf{b}}}{dt} = \Omega \left[-\frac{1}{3} \sin \alpha \cos \phi \left(1 - \frac{1}{2} \sin^2 \theta \right), \frac{2}{3} \frac{\sin \alpha \cos \phi}{\sin \theta}, 0 \right] + O(\sin^3 \theta) \quad (\text{G8})$$

The shift in $\hat{\mathbf{b}}$ due to aberration, (F10), then corresponds to a phase shift of

$$\Delta \Phi = -3 \frac{r}{R_L} \quad (\text{G9})$$

Once this phase shift has been subtracted out, we are left with a remainder

$$\Delta \mathbf{b}' = \frac{r}{R_L} \begin{bmatrix} \frac{5}{3} \cos \alpha \sin \theta - \frac{47}{24} \sin \alpha \cos \phi \sin^2 \theta \\ -\frac{10}{3} \cos \alpha (1 - \frac{33}{40} \sin^2 \theta) + \frac{47}{12} \sin \alpha \cos \phi \sin \theta \\ 0 \end{bmatrix} + O(\sin^3 \theta) \quad (\text{G10})$$

which corresponds to a polarization shift of

$$\Delta \psi' = -\frac{10}{3} \frac{r}{R_L} \cos \alpha \left(1 - \frac{7}{10} \sin^2 \theta \right) + \frac{47}{12} \frac{r}{R_L} \sin \alpha \cos \phi \sin \theta + O(\sin^3 \theta) \quad (\text{G11})$$

REFERENCES

- Barnard, J.J., ApJ, 303, 280.
- Barnard, J.J., & Arons, 1986, ApJ, 302, 138.
- Blaskiewicz, M., Cordes, J.M., & Wasserman, I., 1991, ApJ, 370, 643.
- Chen, K., & Ruderman, M., 1993, ApJ, 408, 179.
- Deutsch, A.J., 1955, Ann. d’Astrophys., 18, 1.

- von Hoensbroech, A., & Xilouris, K.M., 1997, *A&A*, 324, 981.
- Gangadhara, R.T., 1997, *A&A*, 327, 155.
- Gil, J.A. & Lyne, A.G., 1995, *MNRAS*, 276, L55.
- McKinnon, M.M., 1997, *ApJ*, 475, 763.
- McKinnon, M.M., & Stinebring, D.R., 1998, *ApJ*, 502, 883.
- Melatos, A., 1997, *MNRAS*, 288, 1049.
- Navarro, J., 1997, *ApJ*, 486, 1019.
- Radhakrishnan, V., & Cooke, D.J., 1969, *Astrophys. Lett.*, 3, 225.
- Rankin, J., 1990, *ApJ*, 352, 347.
- Xilouris, K.M., et al., 1998, *ApJ*, 501, 286.